Article:

Rigby, S.E., Tyas, A. orcid.org/0000-0001-6078-5215, Clarke, S.D. et al. (1 more author) (2017) Approach to Developing Design Charts for Quantifying the Influence of Blast Wave Clearing on Target Deformation. Journal of Structural Engineering, 143 (1). ISSN 0733-9445

https://doi.org/10.1061/(ASCE)ST.1943-541X.0001626

An Approach to Developing Design Charts for Quantifying the Influence of Blast Wave Clearing on Target Deformation

Sam E. Rigby*, Andrew Tyas†, Sam D. Clarke‡& Ghani Razaqpur§

June 23, 2016

Abstract

If a structural component is located close to the free edge of a building, clearing of the blast wave around the target edge may significantly influence the temporal characteristics of the applied pressure. Because of this, traditional analysis methods assuming a linear decaying load may not be valid, particularly if the blast event imparts a relatively large impulse from the negative phase. Treatment of this phenomenon is brief in the literature, and its influence is usually neglected. This article presents an approach to quantifying the influence of clearing on target deformation, through rigorous analysis of elastic–perfectly-plastic equivalent single-degree-of-freedom (SDOF) systems. The cleared load is evaluated for structural components situated at various distances from the free edge of a reflecting surface using the Hudson acoustic approximation. The results from the SDOF analyses are then used to draw up design charts for determination of the likely influence clearing may have on the design of blast resistant structural components. Four regions are identified: areas where clearing is beneficial; has no effect; is acting adversely; or highly adversely. The method presented herein provides clear demarcation of these regions.

*Lecturer, Department of Civil & Structural Engineering, University of Sheffield, Mappin Street,Sheffield, S1 3JD, UK. Tel.: +44 (0) 114 222 5724. Email: sam.rigby@shef.ac.uk

†Professor & Dstl/RAEng Chair, Department of Civil & Structural Engineering, University of Sheffield, Mappin Street,Sheffield, S1 3JD, UK.

‡Senior Lecturer, Department of Civil & Structural Engineering, University of Sheffield, Mappin Street,Sheffield, S1 3JD, UK.

§Professor, Department of Civil Engineering, McMaster University, JHE-301, 1280 Main Street W.,Hamilton, ON L8S 4L7, Canada

Keywords: Blast; Clearing; Design chart; SDOF

1 Introduction

Designing building components to resist blast loading presents a significant challenge. Typically, the blast load lasts for only a few milliseconds but imparts pressures several orders of magnitude greater than atmospheric pressure, resulting in complex, high strain and high strain-rate response of structural materials. The use of high explosives for malicious attacks has undoubtedly become more common, often with the explosive specifically used to target critical infrastructure. In the majority of high-casualty terrorist attacks the main cause of death is not from the direct effects of the blast itself, but from flying rubble, glass, or building collapse (Dusenberry 2010).

Owing to the difficulties and uncertainties involved with quantifying blast loading, very little formal guidance exists for the design of new protective structures or for the assessment of existing buildings to resist blast loading, particularly when considering that each blast event is effectively a unique combination of an almost infinite spectra of explosive type, mass and charge positioning. The US Department of Defence Design Manual UFC-3-340-02, *Structures to resist the effects of accidental explosions* (US Department of Defence 2008), and the Canadian Design Standard CSA-S850-12, *Design and assessment of buildings subjected to blast loads* (Canadian Standards Association 2012) provide useful guidance for practitioners, however both guides are limited by the fact that they treat the blast load in an overly simplistic manner. In these codes, the blast load is often approximated as a linearly decaying reverse ramp function in order for target deformation to be evaluated from simple 'look-up' charts derived from single-degree-of-freedom (SDOF) analyses (Biggs 1964). This linear load model has been shown to be an inaccurate approximation for certain configurations of charge mass, stand-off and target properties (Gantes & Pnevmatikos 2004), which is of particular importance when considering far-field events where the combined effects of negative phase impulse (Rigby, Tyas, Bennett, Clarke & Fay 2014) and blast wave clearing (Rigby et al. 2012, Rigby, Tyas & Bennett 2014) become dominant factors governing target displacement.

There is the need, therefore, to provide accessible and accurate means for quantifying both the likely effects of phenomena such as blast wave clearing, and the situations where these effects will have significant influence on the design of protective systems. The view is to provide engineers with simple 'look-up' style design charts which will apply corrections to existing methods for evaluating target response, such as the well-established SDOF approach, and to provide clear-cut guidance as to where more sophisticated analysis methods should be sought. This article aims to provide such a resource for the consideration of blast wave clearing.

2 Developing an analysis method: Predicting clearing

2.1 Literature clearing predictions

After an incident shock front, Figure 1(a), impinges on a finite reflecting surface, the incident wave continues unimpeded past the target edge whilst the reflected wave begins to travel back towards the source of the blast, Figure 1(b). This causes diffraction around the free edge, and results in propagation of a rarefaction relief wave across the target face, Figure 1(c). This relief wave is driven by flow conditions that exist as a result of the pressure imbalance between the higher pressure reflected region and the lower pressure incident region. As a clearing wave propagates over any point on the target face, it acts to reduce the pressure and impulse at that point. The magnitude of clearing relief is often sufficient to 'overshoot' the incident pressure (Tyas et al. 2011) resulting in early negative phase pressures, i.e. the pressure acting on the target is lower than the pressure that would exist had the target not been obstructing the incident wave.

Figure 2 shows window damage to the headquarters of the Verdens Gang newspaper, located some 150 m from the centre of the explosion caused by the detonation of a $\sim$950 kg ANFO bomb in Oslo, 2011. This image presents an account of the influence of clearing relief: generally the glazing panels located nearest the sides, top and bottom (note the overhang) of the curtain wall have survived the blast, whilst the glazing panels towards the centre of the curtain wall have failed. This is, presumably, as a direct result of the clearing relief offered by the free edges of the building front. Whilst the blast waveform would have been complicated by the urban environment in which the explosion occurred, the effects of this are likely to have been relatively uniform on the façade, and hence the failure pattern of the glass panels is more than likely due to lesser clearing relief on these central panels. Indeed, this building was separated from the explosive origin by a large outdoor communal space, further suggesting that the blast would have arrived relatively planar. Work by the current authors has shown that the displacement of a finite target subjected to a cleared blast loading function can vary between 40–160% of the displacement of a target loaded by a simplified triangular pulse (Rigby, Tyas & Bennett 2014). It can be argued, therefore, that the effect of clearing relief should be properly quantified when designing building components to resist far-field blast events.

The most well known method for predicting clearing relief can be traced back to the work of Norris et al. (1959). Here, the blast pressure is assumed to decay linearly from the peak reflected pressure to the stagnation pressure (the sum of the incident and drag pressures) over a 'clearing time', and follows the form of the stagnation pressure thereafter. Whilst the exact means for calculating the clearing time differs slightly between sources (US Department of Defence 2008, Kinney & Graham 1985), it is essentially a function of the target size, the sonic velocity of the reflected wave and a factor governing the duration of the clearing phase. This is shown schematically in Figure 3, with more information provided by Rigby (2014).

Crucially, these observations were drawn from blast pressure measurements from large scale blast trials and shock-tube tests conducted in the 1950s, where the reflecting structures were orders of magnitude smaller than the 'length' of the blast wave,where the length of the blast wave is given as the temporal integral of the sonic velocity of the incident pulse over the positive phase duration. For weak shock waves this can be simplified as the product of the two. Hence for these tests the clearing effects would have ceased relatively early on during the positive phase and no 'overshoot' early negative pressures would have been observed. This has recently been investigated by Rigby, Tyas, Bennett, Fay, Clarke & Warren (2014), where a series of numerical analyses were conducted to evaluate the cleared pressure-time history acting on rigid targets of decreasing size. The work showed that if the target was $\sim$250 times smaller than the distance from the blast to the target, then the clearing predictions could be reasonably well predicted by the Norris methodology. For larger sized targets the Norris predictions became meaningless. This highlights an important difference between clearing events from large scale nuclear-style blasts and those from typical smaller sized urban explosions.

The work by Rose & Smith (2000) attempted to provide improved corrections to account for clearing relief, with 'clearing factors' developed to enable the impulse acting on a finite target to be reduced from the fully reflected value according the impulse reduction seen in numerical modelling. This method, however, fails to take into account any temporal characteristics of the clearing load and also neglects the negative phase.

2.2 The Hudson method

Hudson (1955) presented a method for predicting clearing based on approximation of the rarefaction relief wave (propagating along the target face, perpendicular to an exponentially decaying pressure wave) as an acoustic pulse. The report was classified and was only made available to the public in 2005, which may explain why the method has been largely overlooked. In this work, the clearing relief function, p, is presented as pressure contours normalised against the peak incident pressure, $p_{so,max}$, as shown in Figure 4(a).

Hudson's normalised time scale, η, and length scale, δ, are given as

$$\eta = \frac{x}{a_0 t_d} \tag{1}$$

$$\delta = \frac{t}{t_d} - \eta \tag{2}$$

respectively, where x is the distance from the point of interest to the nearest free edge, a_0 is the sonic sound speed in air (assumed to be 340 m/s for weak shocks), t is time, and t_d is the positive phase duration. This enables the clearing function to be evaluated for any point on a finite target. Figure 4(b) shows normalised clearing functions for select values of Hudson's clearing length, η. Once the clearing function is evaluated for a single point, this is simply superimposed with the reflected pressure-time history, determined for example from the Kingery & Bulmash (1984) semi-empirical predictions, or the computer code ConWep (Hyde 1991), to give the cleared pressure at that point.

In order to facilitate his analysis, Hudson made a number of assumptions. Firstly, it was assumed that the blast wave arrives planar and the shock is weak, which Hudson himself deemed reasonable for scaled distances, $Z > 2\text{m/kg}^{1/3}$. The second assumption is that the uncleared (reflected) blast pressure, $p_r(t)$, decays exponentially with a unit decay coefficient, $b = 1$, in the 'modified Friedlander equation'

$$p_r(t) = p_{r,max}\left(1 - \frac{t}{t_d}\right)e^{-b\frac{t}{t_d}} \tag{3}$$

where $p_{r,max}$ is the peak reflected pressure and t and t_d are time and positive phase duration as defined previously. Hudson himself states that *'the errors introduced by a variation* $0.5 < b < 2.0$ *are minor... the effect of variation in b for values near unity is very small, becoming noticeable only as* $b \to 0$ *or as b exceeds 5'* (in the original report, Hudson uses the symbol C to represent the decay coefficient; here it has been changed to b to be consistent with the notation used in this paper). The waveform parameter varies between 2.0 and 0.5 for $4 < Z < 20$ (Kingery & Bulmash 1984), so the Hudson clearing corrections can be used throughout this range without any noticeable error. It was also assumed that no flow conditions existed before the arrival of the blast wave, so the method is only applicable for primary shocks.

2.3 Experimental validation of Hudson clearing predictions

Whilst experimental validation was offered in the original Hudson report, it was not of sufficient quality to be definitive. Tyas et al. (2011) conducted a separate experimental validation on a rigid, finite sized concrete block, with dimensions of the reflecting surface shown in Figure 5. Two pressure gauges (labelled G1 and G2) were embedded flush with the surface of a steel plate which was affixed to the front face of the target, giving two separate validation points. The concrete block was ∼2 m in depth, meaning no clearing waves would arrive from the back of the target during the loading duration.

Whilst the results are not repeated here in full, Figure 6 shows the experimental and predicted pressure-time histories at both gauge locations from a 250 g hemispherical PE4 explosion, 4 m from the target, for two nominally identical tests. Here, clearing relief functions from the two side edges and the top edge of the target were superimposed with the reflected pressure determined from ConWep (Hyde 1991), with full reflected pressure also shown for reference. The relatively large amount of clearing relief can be seen to cause the 'overshoot' early negative pressures at around 9 ms after detonation.

Clearly, a high level of experimental control has been achieved, with near-perfect tracking of the measured waveform and the pressure predictions. The full reflected pressure acts until the arrival of the clearing waves from the top and side edges at 8.2 ms for G1, and the earlier arrival of the clearing wave from the top edge at 7.9 ms for G2. After arrival of the clearing waves, the pressure comprises reflected pressure plus clearing relief. The results demonstrate remarkable accuracy both in arrival time and magnitude of clearing relief, which both may be crucial when considering the dynamic response of flexible systems. Peak impulses were predicted to within 3% for G1 and 5% for G2 across the entire test series (Tyas et al. 2011). ConWep *Loads on Structures* impulse predictions (purporting to include clearing) were between 27 and 57% higher than recorded impulses at G1. The Hudson method, therefore, can be used with confidence when quantifying clearing relief for far-field blast events.

3 Developing an analysis method: Evaluating target response

3.1 The SDOF method and associated design charts

With an established and simple method for predicting the load, we can now focus on developing an analysis method to quantify target response to this load. The equivalent single-degree-of-freedom (SDOF) method involves transforming the distributed properties of a 'real-life' system into single-point equivalent properties. This is achieved through multiplying the mass, m, stiffness, k, and load, F, of the system by the mass and load transformation factors respectively, K_M and K_L (where the stiffness transformation factor is identical to the load transformation factor), to give the single-point equivalent mass, m_e, stiffness, k_e and load, F_e. The transformation factors are derived through equating the work done, kinetic energy and internal strain energy of the real life and distributed systems, by assuming a normalised deflected shape profile as a function of the applied load and support conditions. Therefore, the temporal displacement of the SDOF system exactly matches the displacement at a significant point (e.g. midspan) of the real life system, and energy is conserved between the two models.

The SDOF method is advantageous in that the equivalent properties are easy to determine, and the equation of motion can be solved through explicit time-stepping without the need for costly matrix inversion associated with solving multi-degree systems. Biggs (1964) analysed bilinear elastic–perfectly-plastic SDOF systems under a linear decaying, reverse ramp load function,

$$F_e(t) = \begin{cases} F_{e,max}\left(1 - \dfrac{t}{t_{d,lin}}\right), & t \leq t_{d,lin} \\ 0, & t > t_{d,lin} \end{cases} \tag{4}$$

where $F_{e,max}$ is the peak equivalent force and $t_{d,lin}$ is the duration of the triangular load, as in Figure 7(a). In design, the linear load duration is typically reduced from the empirically determined value in order to preserve the positive phase reflected impulse, i_r, such that $t_{d,lin} = 2i_r/p_{r,max}$, where $p_{r,max}$ is the peak reflected pressure.

The SDOF system has a bilinear elastic–perfectly-plastic resistance function as shown in Figure 7(b). This comprises linear elastic behaviour with equivalent spring resistance $k_e z$ until the elastic deflection limit, z_E, is reached, followed by plastic behaviour with constant equivalent spring resistance, R_u, thereafter. After the peak displacement, z_{max}, is reached, the displacement decreases and the system begins to rebound. When rebounding, the system again behaves elastically until an equivalent spring force of $-R_u$ is attained, whereby the system returns to plasticity.

The equation of motion was solved for various combinations of time ratio, given as $t_{d,lin}/T$, where T is the natural period of the system ($T = 2\pi\sqrt{m_e/k_e}$) and resistance ratio, $R_u/F_{e,max}$. The Biggs maximum response curves are shown in Figure 7(c), where the numbers next to the curves give the value of resistance ratio, $R_u/F_{e,max}$, for that curve. Here, the peak displacement, z_{max}, is normalised against the elastic deflection limit, z_E. If the properties of the system and loading are known, the maximum response can simply be read off the chart. However, if the loading differs largely from a simple linear pulse, then the method may not be valid or accurate.

3.2 Experimental validation of SDOF displacements under a cleared load

To determine the validity of the equivalent SDOF method to model target response to a cleared blast load, Rigby et al. (2013) conducted a series of validation tests. Hemispherical PE4 charges were detonated 6 m away from a finite, rigid reflecting surface with a flexible target embedded within the loaded face, held in place with a small clamping plate (Figure 8). The target plates were 0.835 mm thick mild steel spanning the 305 mm horizontal dimension, with constrained rotations and constrained in-plane displacements at the supports, but free to displace horizontally. The plates were slightly undersized in the vertical dimension to prevent the plate from striking the frame whilst displacing. A laser displacement gauge was pointed at the rear-centre of the target and recorded midspan displacements under the imparted cleared blast load.

SDOF models of the plates were also run. Elastic material properties were used (Young's Modulus $E = 210$ GPa, density $\rho = 7850$ kg/m^3 and Poisson's ratio $\nu = 0.3$), as the plates were not loaded to plasticity. The spatial distribution of loading was evaluated using the Hudson clearing predictions acting on a grid of 64×64 elements, superimposed with the ConWep reflected pressure for each node. This was then converted into an energy equivalent uniform load using the spatial load factor, K_S, and applied to each SDOF model (Rigby et al. 2012). The process was done separately for each charge mass, on account of each test having a different positive phase duration and therefore each point on the target having a slightly different clearing length for each test, despite the physical length being the same.

Figure 9 shows the experimental results and SDOF displacements for 175 g hemispherical PE4 at 6 m. The SDOF model was analysed under both cleared and non-cleared load cases and is able to evaluate the dynamic response of the target to a high level of accuracy: peak displacements were predicted to within 5% across the whole test series (Rigby et al. 2013) for the cleared load case. Here, the strong influence of clearing on plate displacement can be seen. The validation exercise has therefore demonstrated the validity of using a combination of Hudson load predictions and SDOF plate deflections.

4 Clearing response spectra

4.1 Model setup

In order to replicate realistic design-based scenarios, the following decisions were made:

- The SDOF equations of motion were solved for elastic–perfectly-plastic systems in order to be comparable to the maximum response charts of Biggs (1964).

- The cleared load comprised superposition of the reflected pressure and *one* clearing relief function only, corresponding to the distance to the *nearest* free edge. This was done to reduce the number of parameters required in both the analyses and resulting 'look-up' charts.

- The exponential reflected pressure at $Z = 8$ m/kg$^{1/3}$ was selected to be representative of far-field events. At this scaled distance, positive and negative phase impulses are identical and the reflected pressure decay coefficient of 0.86 is close to the unit value assumed in Hudson's approximation.

- The system was solved under the exponential reflected pressure, impulse-preserved linear pressure, and cleared pressure with Hudson's clearing length, η (equation 1) equal to 0.01, 0.1, 0.2, 0.4 and 0.8. Examples of the loading functions are shown in Figure 10.

- Peak values of inward displacement and peak values of rebound displacement were stored for all loading conditions.

- The peak inward and rebound displacements under the cleared load, $z_{max,clear}$ and $z_{min,clear}$, were normalised against the peak displacement under the linear load $z_{max,lin}$ for ease of presentation. Note: the models have different values of t_d/T and $t_{d,lin}/T$ on account of the impulse-preserved reduced duration of the linear load.

- For the clearing load, the value of t_d/T was taken as that of the non-cleared exponential reflected pressure duration, so that the duration of cleared pressure need not be calculated when using the 'look-up' charts.

- The peak pressure, target area, equivalent mass, equivalent stiffness and elastic deformation limit were all set as unity to retain normalised values throughout the analyses.

It has been assumed that the structural component is small in relation to the reflecting surface and the imparted loading is therefore spatially uniform and the blast wave arrives planar. If the Hudson clearing length differs significantly over the span of the loaded member, i.e. $\max(\eta) > 2 \times \min(\eta)$, then a more detailed treatment of the spatially non-uniform distribution of cleared pressures may be required. The charts produced in this article can still be used as a first order approximation, however if the explosion is in the near-field then more sophisticated analysis methods may be required.

At the far-field scaled distance studied in this article, structural damage is unlikely but damage to glazing and light cladding could be significant. The results presented in the following sections could also be used to assess and correct situations where, for example, a panel is designed to resist a full reflected blast load but cannot be tested to these conditions due to being situated in a finite surface in an arena blast trial.

4.2 Results

Figures 11, 12, 13, 14 and 15 show contours of normalised peak displacement, $z_{max,clear}/z_{max,lin}$, against resistance ratio, $R_u/F_{e,max}$, and time ratio, t_d/T, for η =0.01, 0.1, 0.2, 0.4 and 0.8 respectively. Here values of $z_{max,clear}$or$z_{min,clear}/z_{max,lin} \approx 1$ show clearing has little effect; values > 1 suggest clearing is adverse; and values < 1 suggest clearing is acting beneficially. Contours are presented for peak displacement in the inward direction in Figures 11–15(a) and for peak displacement in rebound in Figures 11–15(b).Contour levels of 0.6, 1.0 and 1.4 (where appropriate) are indicated to allow for better identification of adverse/beneficial regions.

These contours can effectively be used as correction factors to apply to the Biggs maximum response calculations shown in Figure 7(c), allowing the engineer to evaluate the peak displacement under the linear load and then simply multiply it by the factor read from the charts presented herein. The two directions of displacement have been compiled separately as specific threat levels may mandate different limits for each of these. If the value of η for the loaded component lies between any of the values for which charts are presented in this article, linear interpolation should be used on values of normalised displacement determined from the nearest values of η.

4.3 Observations and recommendations

It can be seen that for smaller values of η, clearing largely acts beneficially, reducing the displacement to around 50% of the displacement under the linear load. This is most apparent for low values of t_d/T for all resistance ratios, and for high values of t_d/T for lower resistance ratios. At these two extremes, deformation is either entirely elastic or grossly plastic, hence the time taken to reach peak deformation far exceeds the loading duration and the system benefits from the reduction in impulse caused by clearing.

For larger values of η, the elastic benefit of clearing is still realised for low values of t_d/T, however there is no substantial benefit for the peak inward displacement in the grossly plastic zone for high t_d/T, low $R_u/F_{e,max}$ systems as the arrival of the clearing wave is delayed and the target reaches peak deformation before the effects of clearing occur. See, for example, the cleared load for $\eta = 0.4$ in Figure 10. Here, the system experiences the full reflected pressure for $\sim$40% of the positive phase duration.

In this region of high t_d/T and low $R_u/F_{e,max}$ ratios, for all values of η, the peak rebound displacement is (close to) zero and the residual plastic deformation of the plates are in the inward direction.

As with high t_d/T and high $R_u/F_{e,max}$ systems, the effects of clearing are largely negligible because here the quasi-static asymptote is approached and the maximum displacement is mainly influenced by peak pressure. Hence, the results converge to 1.0 with increasing time and resistance ratios, even for $\eta = 0.01$.

Crucially for design purposes, there is a region in the dynamic regime where clearing is acting adversely. Whilst this only results in $\sim$10% greater displacement for lower values of η, the effect rises to over 50% greater displacements for $\eta = 0.8$. This is as a result of negative phase pressures coinciding with target rebound and hence is particularly amplified at $t_d/T \approx 0.25$ (Rigby, Tyas & Bennett 2014). There is also a slight further increase in relative displacement around $R_u/F_{e,max} \approx 0.6$ where the SDOF system under the linear load remains elastic whilst the SDOF system under the cleared load enters plasticity in rebound. This feature is therefore absent on the peak inward displacement charts and is replaced by a sharp drop-off in the normalised displacement, seen in Figures 11, 12, 13, 14 and 15(a) for intermediate values of resistance and time ratios. Here, the reduction in impulse from clearing is sufficient to prevent plasticity occurring on the inward displacement cycle, but the increased (and earlier) negative impulses may cause plasticity in rebound. As the rebound plasticity is not shown in Figures 11, 12, 13, 14 and 15 (a), the sharp demarcation effectively marks the elastic limit of the plates.

The results converge with the fully reflected (non-cleared) case with increasing values of η. It was found that there was no significant difference between the maximum response spectra for $\eta = 0.8$ and $\eta \to \infty$, hence the response spectra for $\eta = 0.8$ can be used to also represent the fully reflected case with no significant loss of accuracy.

4.4 Adverse and beneficial clearing regions

From inspection of Figures 11–15, it appears as though the adverse and beneficial regions of clearing are well defined for larger values of $R_u/F_{e,max}$, where target response is largely elastic with little or no plastic deformation, which in this article is deemed to hold true for $R_u/F_{e,max} \geq 0.8$ for all values of η.

To facilitate the development of a 'look-up' chart, the following regions are defined, which are highlighted by the marked contour levels in Figures 11–15. Values of normalised displacement $z_{max,clear}/z_{max,lin} < 0.6$ are defined as 'beneficial', values between 0.6 and 1.0 are defined as 'no effect', values greater than 1.0 but less than 1.4 are defined as 'adverse', and normalised responses higher than 1.4 are defined as 'highly adverse'. The maximum normalised displacement across the whole response spectra was $\sim$1.6, so this serves as an upper bound, with 0.6 serving as a conservative lower bound. The time ratios of these displacement levels, i.e. the value of t_d/T when the contour line is parallel with the y axis for increasing $R_u/F_{e,max}$, are shown in Table 1.

Simple two-coefficient equations of the form $t_d/T = A \ln \eta + B$ were fit to the data points in Table 1 to enable the adverse and beneficial regions to be evaluated over all values of η. The resulting expressions are shown in Table 2, where separate formulae are presented for $\eta > 0.2$ on account of the introduction of the highly adverse region. Correction factors are also given, which represent the multiplier that should be applied to the peak displacement determined from the linear load model, e.g. the Biggs design charts. The regions are also shown in Figure 16, which, although derived from largely elastic SDOF systems, will be conservative for systems with significant post-elastic behaviour, and hence can still be used for deign purposes.

This method offers a simple means for quantifying the influence of clearing on the response of targets located close to the free edge of a larger reflecting surface. The loading function used in this article is based on consideration of the underling physical processes of the blast pressure and has been validated by well-controlled experimental trials. Aside from its simplicity, the main advantage of using the response spectra presented herein is that they are directly compliant with, and are indeed derived from, the equivalent SDOF method; a widely used analysis technique which is common in design guidance and will be familiar to practising engineers.

5 Worked example

A 4 m long S355 steel 254×254×132 UC section is located 2.5 m from the edge of a building according to the geometry outlined in Figure 17(a). The columns are spaced at 5 m along the front of the building. A 15 kg hemisphere of TNT is detonated at ground level, 16 m from the centreline of the column. The column is simply supported and has Young's modulus, density, and yield strength of 200 GPa, 7850 kg/m^3 and 355 MPa respectively. The dimensions of the column section are shown in Figure 17(b), with dynamic properties given in table 3. The column can be assumed to behave as elastic–perfectly-plastic. Determine the maximum displacement of the column.

5.1 Step 1: Calculate blast parameters

- $R = 16$ m, $W = 15$ kg, $Z = 6.49$ m/kg$^{1/3}$
- Max angle of incidence $\theta = \cos^{-1}\left(16/\sqrt{16^2 + 4^2 + 2.5^2}\right) = 16.4°$
- As the blast will impinge on the column's supported area at small angles of incidence we can use normally reflected values from ConWep
- $p_{r,max} = 62.17$ kPa, $i_r = 233$ kPa.ms, $t_d = 10.25$ ms.

5.2 Step 2: Calculate linear SDOF displacement

- Column is uniformly loaded and simply supported: $K_L = 0.64$, $K_M = 0.50$ Morison (2007)
- Calculate peak equivalent force: $F_{e,max} = p_{r,max} \times K_L \times L \times \text{column spacing} = 62.17 \times 0.64 \times 4 \times 5 = 796$ kN

- $R_u/F_{e,max} = 0.64 \times 1157.8/796 = 0.931$
- Calculate linear duration: $t_{d,lin} = 2i_r/p_{r,max} = 2 \times 233/62.17 = 7.5$ ms
- Calculate linear time ratio: $t_{d,lin}/T = 7.5/17.4 = 0.432$
- Read maximum displacement from Figure 7(c): $z_{max}/z_E = 1.212$
- Therefore $z_{max,lin} = 1.212 \times 21.4 = 26$ mm.

5.3 Step 3: Calculate displacement under cleared load

- Calculate clearing length: $\eta = x/a_0 t_d = 2.5/(340 \times 0.01025) = 0.72$
- $R_u/F_{e,max} > 0.8$ therefore can use simplified clearing factors in Figure 16
- Calculate time ratio: $t_d/T = 10.25/17.3 = 0.59$
- Read clearing factor from Figure 16 for $\eta = 0.7$ and $t_d/T = 0.6$: clearing factor = 1.4
- $z_{max,clear} = z_{max,lin} \times$ clearing factor $= 26 \times 1.4 = 36.4$ mm
- Consideration of the combined effects of clearing and the negative phase results in greater levels of plasticity, and hence clearing should not be neglected for the design of this column.

6 Summary and conclusions

This article presents the development of maximum response spectra charts for quantifying the influence of blast wave clearing on target deformation.

Clearing, caused by diffraction of a blast front around a target edge, is known to reduce the impulse acting on a loaded target, and can often 'overshoot' the incident pressure and bring about early negative phase pressures. This may have a significant impact on the displacement of targets which are sensitive to the time-varying form of the applied pressure load.

The Hudson (1955) method is introduced, which provides a physically valid basis for approximating the cleared pressure. Previous experimental validation work of Tyas et al. (2011) is summarised, which demonstrated excellent agreement with the cleared pressure predictions.

The equivalent SDOF method (Biggs 1964) allows a distributed system to be modelled as a single-point equivalent. Rigby et al. (2013) conducted dynamic experiments on finite-sized targets subjected to cleared blast loads and modelled the target response using an SDOF model loaded by the Hudson corrected cleared load function. Again, the results demonstrated excellent agreement and confirmed the validity of the method.

This approach was then extended to study the effects of clearing and to draw up design charts for quantifying the effect through rigorous analysis of elastic–perfectly-plastic equivalent SDOF systems. It was found that clearing is largely beneficial for impulsive systems, and has little effect for quasi-static systems, unless the strength of the target is low compared to the applied pressure *and* the target is located close to the free edge, whereby some benefit may be gained from clearing. It was also shown that displacements could be over 50% greater when considering clearing as opposed to a simple linear load on account of the negative pressures coinciding with target rebound.

Response spectra charts are offered as a simple means for correcting the displacement determined from analysis methods assuming a linear decaying load. These response spectra are finally condensed into a simple chart which allows easy determination of the likely effect of clearing, and requires only the time ratio, t_d/T, and Hudson clearing length, η, to be calculated. The method has clear strengths in terms of its simplicity, accuracy, and physical validity, and is imminently useful for practicing engineers.

It was found that dynamic response under a cleared load will fall into one of four categories, namely regions where clearing is beneficial; is acting adversely; is acting highly adversely; or has no effect. These regions are demarcated in Figure 16 and Table 2, with correction factors of 0.6, 1.4, 1.6 and 1.0 suggested for response in each of the regions respectively.

Finally, a worked example is provided to demonstrate how the method would work in practice.

References

Biggs, J. M. (1964), *Introduction to Structural Dynamics*, McGraw-Hill, New York, NY, USA.

Canadian Standards Association (2012), *Design and assessment of buildings subjected to blast loads*, CSA Group, Mississauga, Canada, CSA-S850-12.

Dusenberry, D. O. (2010), *Handbook for blast-resistant design of buildings*, John Wiley & Sons, Hoboken, NJ, USA.

Gantes, C. & Pnevmatikos, N. (2004), 'Elastic-plastic response spectra for exponential blast loading', *International Journal of Impact Engineering* **30**(3), 323–343.

Hudson, C. C. (1955), Sound pulse approximations to blast loading (with comments on transient drag), Technical Report SC-TM-191-55-51, Sandia Corporation, MD, USA.

Hyde, D. W. (1991), *Conventional Weapons Program (ConWep)*, U.S Army Waterways Experimental Station, Vicksburg, MS, USA.

Kingery, C. N. & Bulmash, G. (1984), Airblast parameters from TNT spherical air burst and hemispherical surface burst, Technical Report ARBRL-TR-02555, U.S Army BRL, Aberdeen Proving Ground, MD, USA.

Kinney, G. F. & Graham, K. J. (1985), *Explosive Shocks in Air*, Springer, NY, USA.

Morison, C. (2007), The resistance of laminated glass to blast pressure loading and the coefficients for single degree of freedom analysis of laminated glass, PhD thesis, Defence College Management and Technology, Cranfield University, UK.

Norris, C. H., Hansen, R. J., Myle, J. H., Biggs, J. M., Namyet, S. & Minami, J. K. (1959), *Structural Design for Dynamic Loads*, McGraw-Hill, New York, NY, USA.

Rigby, S. E. (2014), Blast Wave Clearing Effects on Finite-Sized Targets Subjected to Explosive Loads, PhD thesis, Department of Civil and Structural Engineering, University of Sheffield, UK.

Rigby, S. E., Tyas, A. & Bennett, T. (2012), 'Single-degree-of-freedom response of finite targets subjected to blast loading - the influence of clearing', *Engineering Structures* **45**, 396–404.

Rigby, S. E., Tyas, A. & Bennett, T. (2014), 'Elastic-plastic response of plates subjected to cleared blast loads', *International Journal of Impact Engineering* **66**, 37–47.

Rigby, S. E., Tyas, A., Bennett, T., Clarke, S. D. & Fay, S. D. (2014), 'The negative phase of the blast load', *International Journal of Protective Structures* **5**(1), 1–20.

Rigby, S. E., Tyas, A., Bennett, T., Fay, S. D., Clarke, S. D. & Warren, J. A. (2014), 'A numerical investigation of blast loading and clearing on small targets', *International Journal of Protective Structures* **5**(3), 523–574.

Rigby, S. E., Tyas, A., Bennett, T., Warren, J. A. & Fay, S. (2013), 'Clearing effects on plates subjected to blast loads', *Engineering and Computational Mechanics* **166**(3), 140–148.

Rose, T. A. & Smith, P. D. (2000), An approach to the problem of blast wave clearing on finite structures using empirical procedures based on numerical calculations, *in* '16th Symposium on the Military Aspects of Blast and Shock (MABS16)', Oxford, UK, pp. 113–120.

Tyas, A., Warren, J., Bennett, T. & Fay, S. (2011), 'Prediction of clearing effects in far-field blast loading of finite targets', *Shock Waves* **21**(2), 111–119.

US Department of Defence (2008), *Structures to resist the effects of accidental explosions*, US DoD, Washington DC, USA, UFC-3-340-02.

List of Figures

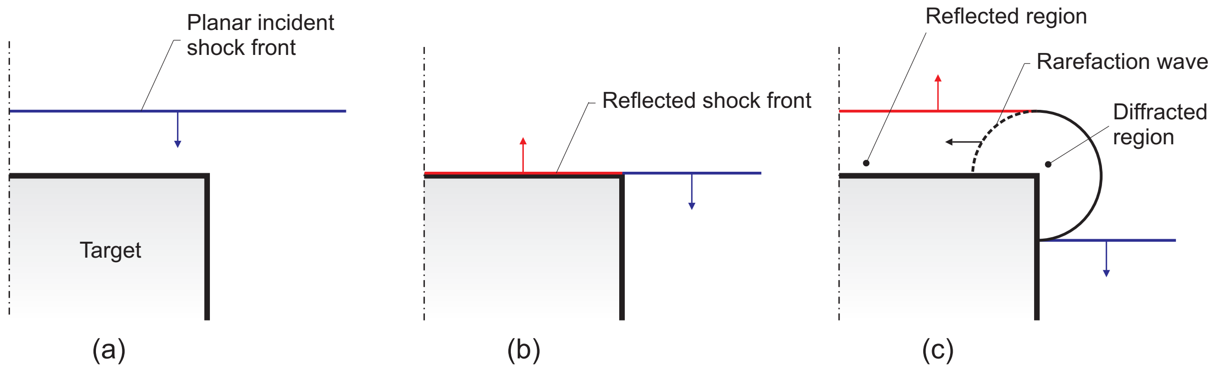

Figure 1: Diffraction of a blast wave around a finite target causing the propagation of a rarefaction clearing wave (Rigby 2014)

Figure 2: Window damage after the 2011 Oslo bombings (© Andreas Lunde/Demotix)

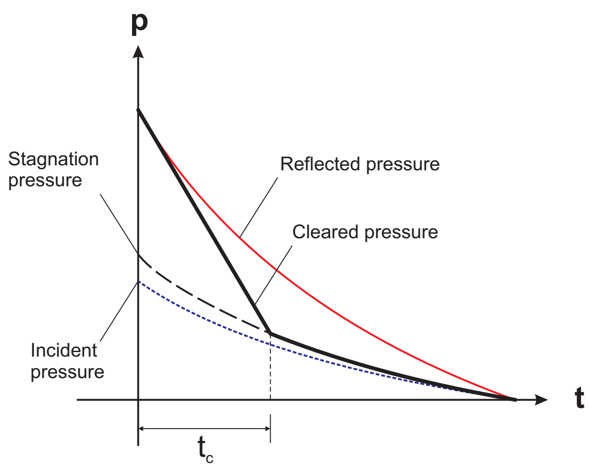

Figure 3: Empirical clearing corrections, after Norris et al. (1959)

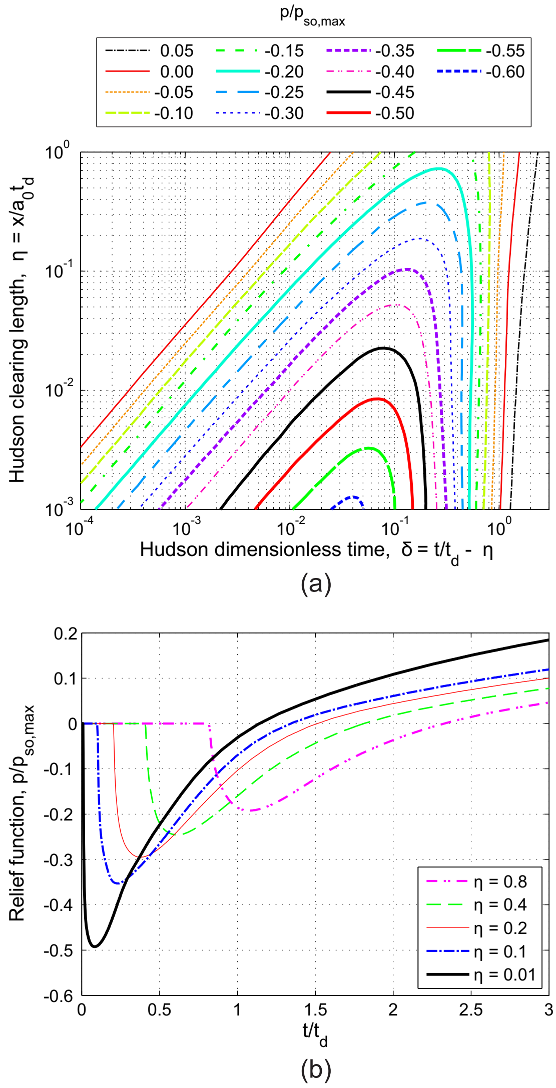

Figure 4: (a) Normalised pressure contours for the Hudson (1955) clearing relief function, (b) Hudson clearing functions for select values of η

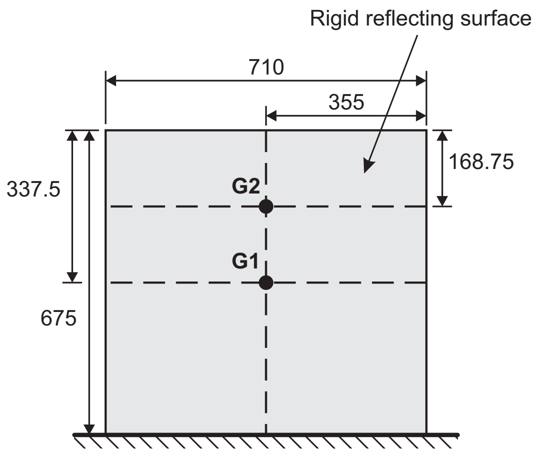

Figure 5: Dimensions of the finite reflecting surface (mm) used for the pressure validation tests (Tyas et al. 2011)

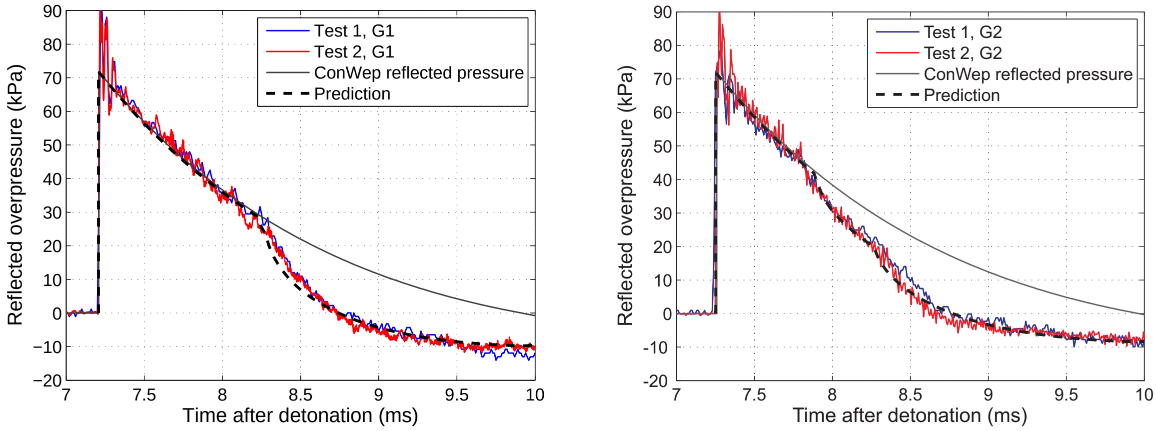

(a) G1

(b) G2

Figure 6: Validation of Hudson clearing predictions (Tyas et al. 2011)

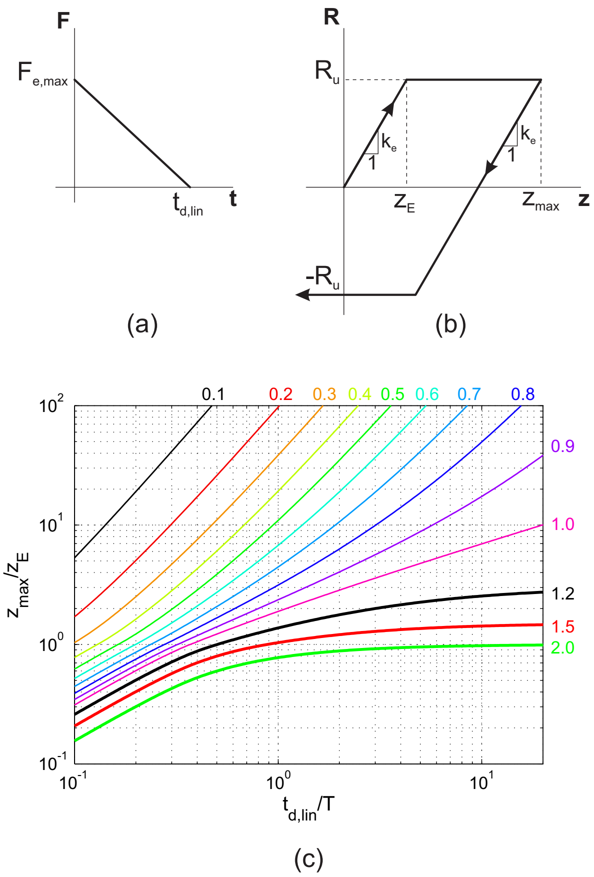

Figure 7: (a) Triangular load-time history, (b) resistance-deflection function, (c) maximum deflection of an elastic–perfectly-plastic SDOF system under a triangular load (Biggs 1964) – numbers next to curves are resistance ratio, $R_u/F_{e,max}$

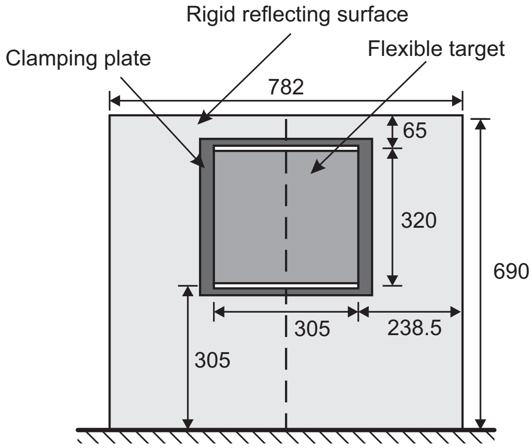

Figure 8: Dimensions of the finite reflecting surface (mm) used for the displacement validation tests (Rigby et al. 2013)

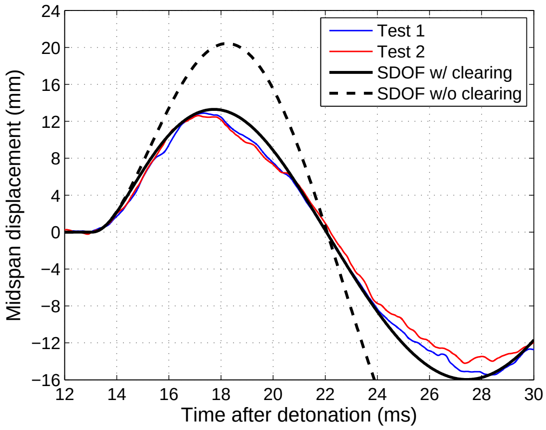

Figure 9: Experimental and SDOF displacements for 175 g hemispherical PE4 at 6 m

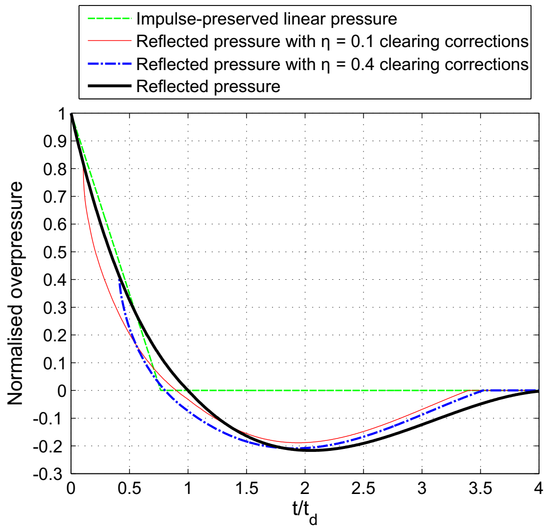

Figure 10: Pressures applied to the numerical model

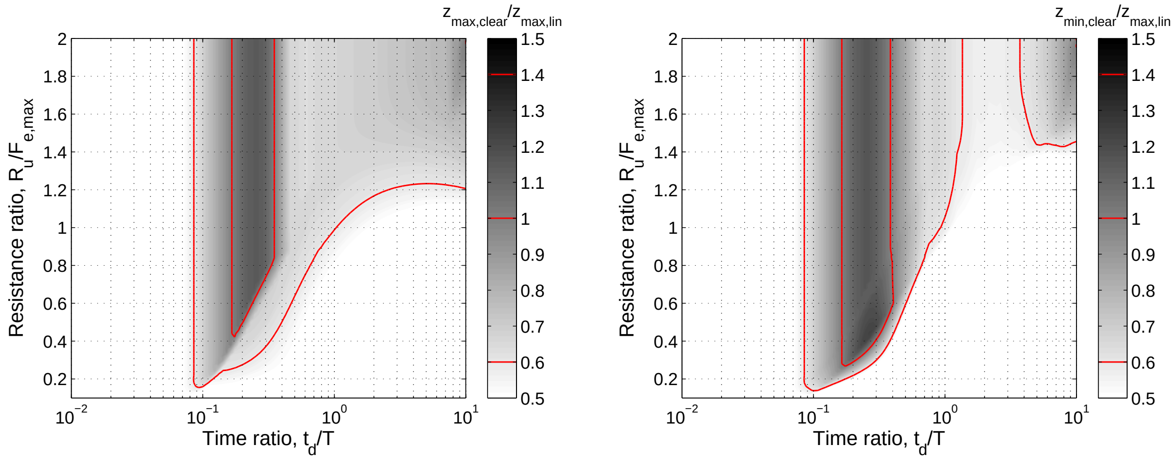

(a) Peak inward displacement

(b) Peak rebound displacement

Figure 11: Normalised peak deformation spectra for $\eta = 0.01$

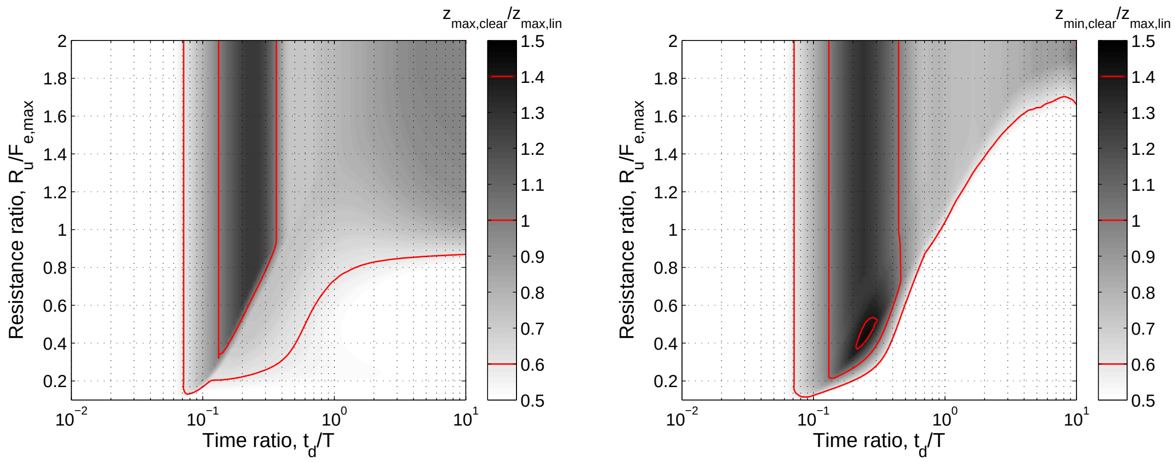

(a) Peak inward displacement

(b) Peak rebound displacement

Figure 12: Normalised peak deformation spectra for $\eta = 0.1$

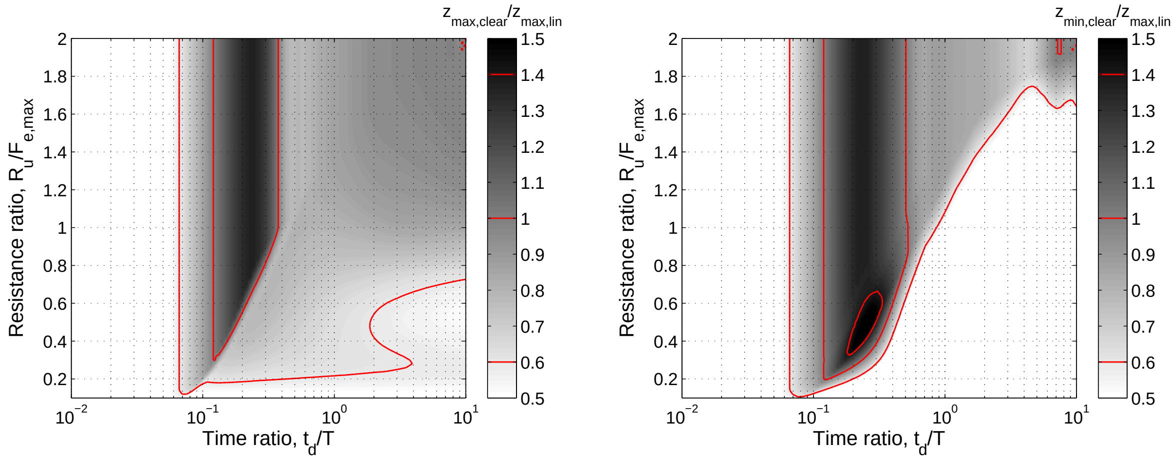

(a) Peak inward displacement (b) Peak rebound displacement

Figure 13: Normalised peak deformation spectra for $\eta = 0.2$

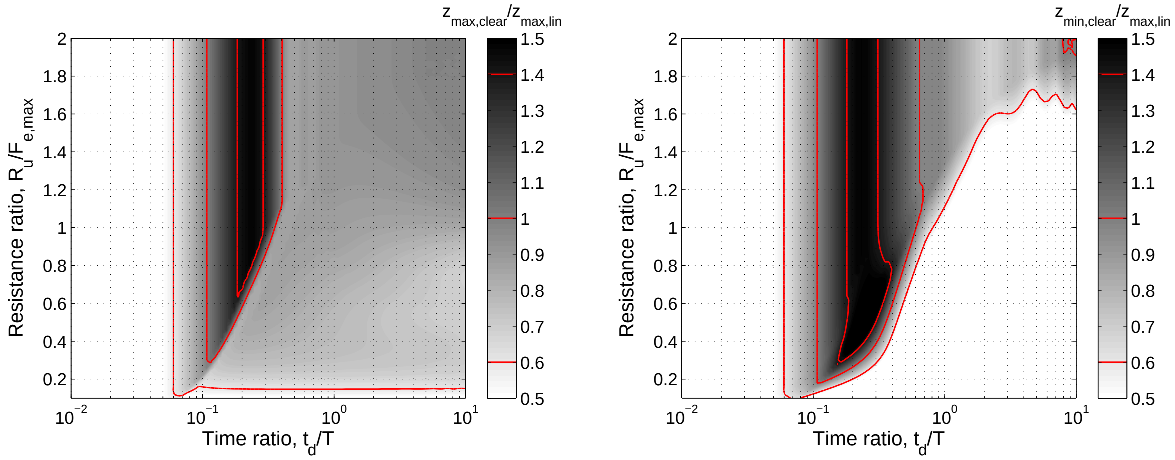

(a) Peak inward displacement

(b) Peak rebound displacement

Figure 14: Normalised peak deformation spectra for $\eta = 0.4$

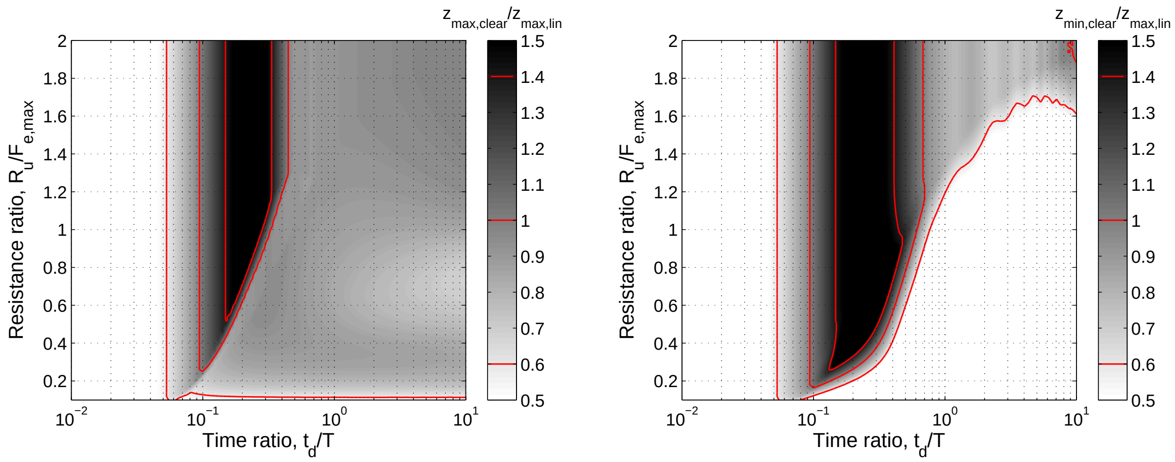

(a) Peak inward displacement

(b) Peak rebound displacement

Figure 15: Normalised peak deformation spectra for $\eta = 0.8$

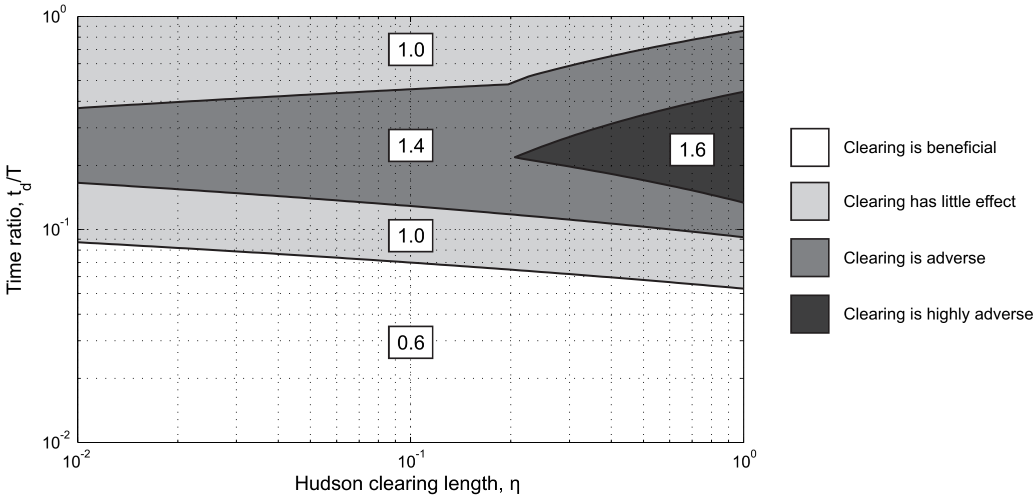

Figure 16: Regions of adverse and beneficial behaviour when considering clearing, with correction factors given for each region

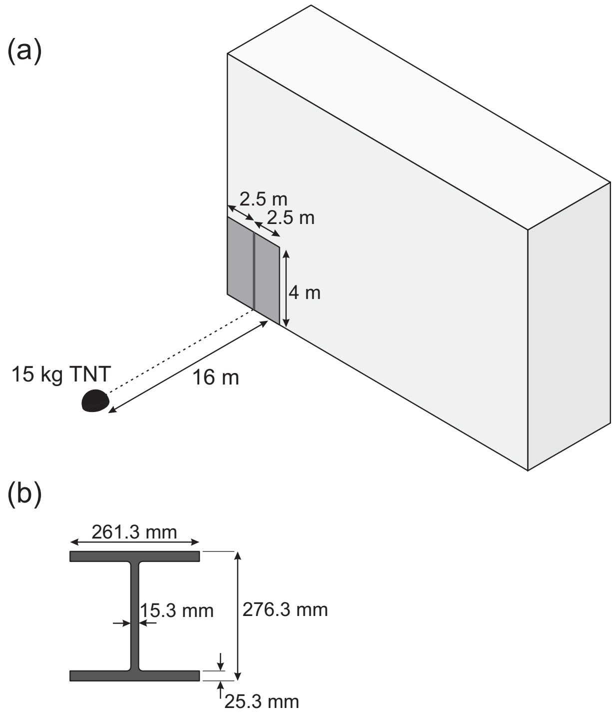

Figure 17: (a) Geometry of the worked example, (b) dimensions of 254×254×132 UC section

List of Tables

η	t_d/T				
	$z_{max,clear}/z_{max,lin}$				
	0.6	1.0	1.4	1.4	1.0
0.01	0.0851	0.1644	-	-	0.3843
0.1	0.0712	0.1309	-	-	0.4437
0.2	0.0659	0.1196	-	-	0.5048
0.4	0.0599	0.1072	0.1804	0.3105	0.6435
0.8	0.0529	0.0938	0.1473	0.4095	0.6811

Table 1: Tabulated values of t_d/T at specific contour levels of $z_{max,clear}/z_{max,lin}$

Clearing length	Inequality			Region	Correction factor
$\eta \leq 0.2$		t_d/T	$< -0.0075\ln\eta + 0.0527$	Beneficial	0.6
	$-0.0075\ln\eta + 0.0527 \leq$	t_d/T	$< -0.0162\ln\eta + 0.0919$	No effect	1.0
	$-0.0162\ln\eta + 0.0919 \leq$	t_d/T	$< +0.0365\ln\eta + 0.5394$	Adverse	1.4
	$+0.0365\ln\eta + 0.5394 \leq$	t_d/T		No effect	1.0
$0.2 < \eta \leq 1.0$		t_d/T	$< -0.0075\ln\eta + 0.0527$	Beneficial	0.6
	$-0.0075\ln\eta + 0.0527 \leq$	t_d/T	$< -0.0162\ln\eta + 0.0919$	No effect	1.0
	$-0.0162\ln\eta + 0.0919 \leq$	t_d/T	$< -0.0528\ln\eta + 0.1336$	Adverse	1.4
	$-0.0528\ln\eta + 0.1336 \leq$	t_d/T	$< +0.1424\ln\eta + 0.4435$	Highly adverse	1.6
	$+0.1424\ln\eta + 0.4435 \leq$	t_d/T	$< +0.2246\ln\eta + 0.8570$	Adverse	1.4
	$+0.2246\ln\eta + 0.8570 \leq$	t_d/T		No effect	1.0

Table 2: Tabulated regions of adverse and beneficial clearing behaviour with associated correction factor (if $\eta > 1$, use $\eta = 1.0$)

Parameter	Symbol	Value (unit)
Young's modulus	E	200 (GPa)
Density	ρ	7850 (kg/m^3)
Yield strength	σ_y	355 (MPa)
Load factor	K_L	0.64 (-)
Mass factor	K_M	0.50 (-)
Spring constant	k	384/5 (-)
Span	L	4 (m)
Cross-sectional area	A	0.0168 (m^2)
Elastic section modulus	Z_x	1631 (cm^2)
Second moment of area	I_{xx}	22530 (cm^4)
Stiffness	K	54072 (kN/m)
Mass	M	527.5 (kg)
Equivalent stiffness	K_e	34606 (kN/m)
Equivalent mass	K_e	263.7 (kg)
Equivalent elastic resistance	R_u	1157.8$\times K_L$ (kN)
Elastic limit	z_E	21.4 (mm)
Natural period	T	17.3 (ms)

Table 3: Dynamic properties for a 4 m long S355 steel 254×254×132 UC section pinned at both ends